NASA/CR-2002-211760
ICASE Report No. 2002-27

Constitutive Modeling of Nanotube-reinforced Polymer Composites

G.M. Odegard
ICASE, Hampton, Virginia

T.S. Gates
NASA Langley Research Center, Hampton, Virginia

K.E. Wise and C. Park
ICASE, Hampton, Virginia

E.J. Siochi
NASA Langley Research Center

July 2002

Report Documentation Page

Report Date	Report Type	Dates Covered (from... to)
00JUL2002	N/A	-

Title and Subtitle Constitutive Modeling of Nanotube-reinforced Polymer Composites	**Contract Number**
	Grant Number
	Program Element Number
Author(s) G.M. Odegard, T.S. Gates, K.E. Wise, C. Park, and E.J. Siochi	**Project Number**
	Task Number
	Work Unit Number
Performing Organization Name(s) and Address(es) ICASE Mail Stop 132C NASA Langley Research Center Hampton, VA 23681-2199	**Performing Organization Report Number**
Sponsoring/Monitoring Agency Name(s) and Address(es)	**Sponsor/Monitor's Acronym(s)**
	Sponsor/Monitor's Report Number(s)

Distribution/Availability Statement
Approved for public release, distribution unlimited

Supplementary Notes
ICASE Report No. 2002-27

Abstract
see report

Subject Terms

Report Classification unclassified	**Classification of this page** unclassified
Classification of Abstract unclassified	**Limitation of Abstract** SAR

Number of Pages
36

The NASA STI Program Office . . . in Profile

Since its founding, NASA has been dedicated to the advancement of aeronautics and space science. The NASA Scientific and Technical Information (STI) Program Office plays a key part in helping NASA maintain this important role.

The NASA STI Program Office is operated by Langley Research Center, the lead center for NASA's scientific and technical information. The NASA STI Program Office provides access to the NASA STI Database, the largest collection of aeronautical and space science STI in the world. The Program Office is also NASA's institutional mechanism for disseminating the results of its research and development activities. These results are published by NASA in the NASA STI Report Series, which includes the following report types:

- TECHNICAL PUBLICATION. Reports of completed research or a major significant phase of research that present the results of NASA programs and include extensive data or theoretical analysis. Includes compilations of significant scientific and technical data and information deemed to be of continuing reference value. NASA's counterpart of peer-reviewed formal professional papers, but having less stringent limitations on manuscript length and extent of graphic presentations.

- TECHNICAL MEMORANDUM. Scientific and technical findings that are preliminary or of specialized interest, e.g., quick release reports, working papers, and bibliographies that contain minimal annotation. Does not contain extensive analysis.

- CONTRACTOR REPORT. Scientific and technical findings by NASA-sponsored contractors and grantees.

- CONFERENCE PUBLICATIONS. Collected papers from scientific and technical conferences, symposia, seminars, or other meetings sponsored or cosponsored by NASA.

- SPECIAL PUBLICATION. Scientific, technical, or historical information from NASA programs, projects, and missions, often concerned with subjects having substantial public interest.

- TECHNICAL TRANSLATION. English-language translations of foreign scientific and technical material pertinent to NASA's mission.

Specialized services that complement the STI Program Office's diverse offerings include creating custom thesauri, building customized data bases, organizing and publishing research results . . . even providing videos.

For more information about the NASA STI Program Office, see the following:

- Access the NASA STI Program Home Page at ***http://www.sti.nasa.gov***

- Email your question via the Internet to help@sti.nasa.gov

- Fax your question to the NASA STI Help Desk at (301) 621-0134

- Telephone the NASA STI Help Desk at (301) 621-0390

- Write to:
  NASA STI Help Desk
  NASA Center for AeroSpace Information
  7121 Standard Drive
  Hanover, MD 21076-1320

NASA/CR-2002-211760
ICASE Report No. 2002-27

Constitutive Modeling of Nanotube-reinforced Polymer Composites

G.M. Odegard
ICASE, Hampton, Virginia

T.S. Gates
NASA Langley Research Center, Hampton, Virginia

K.E. Wise and C. Park
ICASE, Hampton, Virginia

E.J. Siochi
NASA Langley Research Center

ICASE
NASA Langley Research Center
Hampton, Virginia
Operated by Universities Space Research Association

Prepared for Langley Research Center
under Contract NAS1-97046

July 2002

Available from the following:

NASA Center for AeroSpace Information (CASI)
7121 Standard Drive
Hanover, MD 21076-1320
(301) 621-0390

National Technical Information Service (NTIS)
5285 Port Royal Road
Springfield, VA 22161-2171
(703) 487-4650

CONSTITUTIVE MODELING OF NANOTUBE-REINFORCED POLYMER COMPOSITES

G.M. ODEGARD[1], T.S. GATES[2], K.E. WISE[1], C. PARK[1], and E.J. SIOCHI[3]

Abstract. In this study, a technique is presented for developing constitutive models for polymer composite systems reinforced with single-walled carbon nanotubes (SWNT). Because the polymer molecules are on the same size scale as the nanotubes, the interaction at the polymer/nanotube interface is highly dependent on the local molecular structure and bonding. At these small length scales, the lattice structures of the nanotube and polymer chains cannot be considered continuous, and the bulk mechanical properties can no longer be determined through traditional micromechanical approaches that are formulated by using continuum mechanics. It is proposed herein that the nanotube, the local polymer near the nanotube, and the nanotube/polymer interface can be modeled as an effective continuum fiber using an equivalent-continuum modeling method. The effective fiber serves as a means for incorporating micromechanical analyses for the prediction of bulk mechanical properties of SWNT/polymer composites with various nanotube lengths, concentrations, and orientations. As an example, the proposed approach is used for the constitutive modeling of two SWNT/polyimide composite systems.

Key words. carbon nanotubes, composites, mechanical properties, modeling, nanotechnology

Subject classification. Structures and Materials

Nomenclature

Molecular model

a	-Bond number
D_a^{IJ}	-Well depth of interaction a involving atoms I and J
K_a^{θ}	-Angle variance force constant
K_a^{ρ}	-Stretching force constant
Λ^{m}	-Total molecular potential energy
θ_a	-Deformed bond-angle number a
Θ_a	-Undeformed bond-angle number a
ρ_a	-Deformed interatomic distance of bond number a
ρ_a^{IJ}	-Van der Waals distance for interaction a involving atoms I and J
P_a	-Undeformed interatomic distance of bond number a

Equivalent-truss model

A_a^b	-Cross-sectional area of rod a of truss member type b
r_a^b	-Deformed lengths of rod a of truss member type b

[1] ICASE, MS 132C, NASA Langley Research Center, Hampton, VA 23681. This research was partially supported by the National Aeronautics and Space Administration under NASA Contract No. NAS1-97046 while Dr. Odegard, Dr. Wise, and Dr. Park were in residence at ICASE, NASA Langley Research Center, Hampton, VA 23681-2199.

[2] Mechanics and Durability Branch, MS 188E, NASA Langley Research Center, Hampton, VA 23681

[3] Advanced Materials and Processing Branch, MS 226, NASA Langley Research Center, Hampton, VA 23681

R_a^b -Undeformed lengths of rod *a* of truss member type *b*
Y_a^b -Young's modulus of rod *a* of truss member type *b*
α -Bond-stretching interaction truss member type
β -Bond-angle variance interaction truss member type
Λ^t -Total strain energy of truss model
ω -Van der Waals interaction truss member type

Equivalent-continuum model and composite

$\mathbf{A}^f$ -Dilute mechanical strain concentration tensor of effective fiber
c_{ij} -Directions cosines for coordinate transformation
$\mathbf{C}$ -Elastic stiffness tensor of the composite
C_{ijkl}^f, C_{ij}^f, $\mathbf{C}^f$ -Elastic stiffness tensor of effective fiber
$\mathbf{C}^m$ -Elastic stiffness tensor of matrix
D -Diameter of effective fiber
e -Applied strain magnitude
E -Young's modulus of isotropic anisotropic composite
E_L -Longitudinal Young's modulus of composite
E_T -Transverse Young's modulus of anisotropic composite
E_L^f -Longitudinal Young's modulus of effective fiber
G -Shear modulus of isotropic composite
G_L -Longitudinal shear modulus of anisotropic composite
G_L^f -Longitudinal shear modulus of effective fiber
G_T^f -Transverse shear modulus of effective fiber
$\mathbf{I}$ -Identity tensor
k -Axisymmetric alignment factor
K_T^f -Transverse bulk modulus of effective fiber
L -Length of effective fiber
n_j -Outward normal to boundary *B*
s_1, s_2 -Orientation factors
$\mathbf{S}$ -Eshelby's tensor
$T_i(B)$ -Tractions applied onto boundary *B*
$u_i(B)$ -Displacements applied onto boundary *B*
v_f -Effective fiber volume fraction
v_m -Matrix volume fraction
V -Volume of effective fiber
x_j -Coordinate system of effective fiber
x_j''' -Global coordinate system
ε_{kl} -Strain tensor
$\delta(y-\overline{y})$ -Dirac delta distribution centered at $\overline{y}$
ϕ, ψ, γ -Angles of coordinate transformation
$\lambda(\phi,\psi)$ -Orientation distribution function
Λ^f -Total strain energy of effective fiber
σ_{ij} -Stress tensor

1. Introduction. In recent years, nano-structured, non-metallic materials have spurred considerable interest in the materials community partly due to their potential for large gains in mechanical and physical

properties as compared to standard structural materials. In particular, carbon nanotube-reinforced polymer composites may provide order-of-magnitude increases in strength and stiffness when compared to typical carbon-fiber reinforced polymeric composites. In order to facilitate the development of nanotube-reinforced polymer composites, constitutive relationships must be developed that predict the bulk mechanical properties of the composite as a function of molecular structure of the polymer, nanotube, and polymer/nanotube interface.

For computational simplicity and to adequately address scale-up issues, it is desirable to couple an equivalent-continuum model of a nanotube/polymer composite with established micromechanical models to describe the mechanical behavior. As outlined by McCullough [1, 2], numerous micromechanical models have been developed to predict the macroscopic behavior of polymeric composite materials reinforced with typical reinforcement such as carbon or glass fibers. These micromechanical models assume that the fiber, matrix, and sometimes, the interface, are continuous materials and the constitutive equations for the bulk composite material are formulated based on assumptions of continuum mechanics. However, for nanostructured materials such as nanotube reinforced polymers, a typical single-walled nanotube (SWNT) may have a diameter of approximately $1\text{-}10\times10^{-9}$ meters compared to the typical carbon-fiber diameter of 50×10^{-6} meters leading to a breakdown of the rules and requirements for continuum modeling. Even though a limited number of studies have attempted to address the applicability of continuum micromechanics to nanotube-reinforced polymer composites [3, 4], it appears that the direct use of micromechanics for nanotube composites is inappropriate without taking in account the effects associated with the significant size difference between a nanotube and a typical carbon fiber, as described below.

To help address this problem, atomistic simulation can be used to investigate behavior of materials at the nanometer length scale. Recently, Wise and Hinkley [5] used molecular dynamics simulations to address the polymer/SWNT material response for a SWNT surrounded by polyethylene molecules. They predicted that the local changes in the polymer molecular structure and the non-functionalized polymer/SWNT interface are on the same length-scale as the width of the nanotube. The magnitude of this localized effect is generally unknown and needs to be accurately modeled to ensure that the full load-transfer capabilities of the polymer/SWNT composite are accounted for in both bulk stiffness and strength calculations.

The first step towards calculation of bulk stiffness and strength is to establish a constitutive model that can be used in a continuum mechanics formulation. The continuum model must account for the fundamental assumption in continuum mechanics that the mass, momentum, and energy can be represented in a mathematical sense by continuous functions, that is, independent of length scale.

In this paper, a technique for developing constitutive models for SWNT-reinforced polymer composite materials is proposed which is based on extensions of the equivalent-continuum modeling technique developed by Odegard *et al*. [6]. The modeling technique takes into account the discrete nature of the atomic interactions at the nanometer length scale and the interfacial characteristics of the nanotube and the surrounding polymer matrix. After the constituent materials used in this paper are discussed in detail, the development of the constitutive model using the presented technique is described. First, a model of the molecular structure of the nanotube and the adjacent polymer chains is established by using the atomic structure that has been determined from molecular dynamics (MD) simulations. Second, an equivalent-continuum model is developed in which the mechanical properties are determined based on the force constants that describe the bonded and non-bonded interactions of the atoms in the molecular model and reflect the local polymer and nanotube structure. Finally, the equivalent-continuum model is used in micromechanical analyses to determine the bulk elastic stiffness constitutive properties of the SWNT/polymer composite with aligned and random nanotube orientations and with various nanotube

lengths and volume fractions. In addition, predicted values of modulus are compared with experimental data obtained from mechanical testing.

2. Constituent materials. The constitutive models developed in this study are for SWNT/polyimide composites with a PmPV interface. The properties of the constituent materials are described below.

2.1. Carbon nanotube. In 1991 Iijima [7] obtained transmission electron micrographs of elongated, nano-sized carbon particles that consisted of cylindrical graphitic layers, known today as carbon nanotubes. Because of their high inter-atomic bond strength and perfect lattice structure, a Young's modulus as high as 1 TPa and a tensile strength approaching 100 GPa have been measured for single-walled carbon nanotubes (SWNT) [8]. These properties, in addition to their relatively low density, make SWNT an ideal candidate as a reinforcing constituent. For this study, a (6,6), straight, finite length, single-walled carbon nanotube is modeled.

2.2. Nanotube/polymer interface. Accurate representation of the nanotube to polymer interface is essential for modeling nano-scale structure property relationships. In a recent molecular dynamics study of SWNT/polymer materials, Frankland *et al.* [9] addressed the effects of covalent bonds at the SWNT/polymer interface. They have shown that for nanotube/polyethylene composites there is a one to two order-of-magnitude increase in the interfacial shear strength for composites with covalent bonding between the nanotube and adjacent polymer molecules relative to systems without the covalent bonds. However, other studies [10, 11] have shown that because the covalent bonding may significantly affect the properties of the nanotube itself, it is desirable to increase the load transfer between the nanotube and polymer by using improved non-covalent bonding methods. For example, it has been shown that PmPV molecules [poly(m-phenylenevinylene) substituted with octyloxy chains] naturally wrap around carbon nanotubes in a helical pattern [11]. This wrapping allows for an improved nanotube/polymer molecule interaction through non-covalent bonded interactions, and thus improved load transfer at the nanotube/polymer interface, compared to those found with traditional structural polymers. Because the PmPV polymer molecules will likely entangle themselves with neighboring structural polymer molecules (such as polyimides), the PmPV can be used as a highly effective interface between the nanotube and structural polymer, and is used as the interface in the present study. The molecular structure of a single unit of the PmPV molecule is shown in Fig. 2. The subscripts on the atomic labels in Fig. 2 correspond to the subscripts shown in Tables 1-3, which are discussed below.

2.3. Polymer matrix. The nanotubes used in this study are assumed to be well dispersed inside a bulk polymer matrix. The first polymer considered is LaRC-SI, a thermoplastic polyimide that has been shown to have good mechanical properties for various processing and testing conditions [12-15]. The properties of LaRC-SI used in this study have been taken from Whitley *et al.* [15] for the system with a 3% stoichiometric imbalance at room temperature. The Young's modulus and Poisson's ratio of this material are 3.8 GPa and 0.4, respectively.

The second polymer considered in this study is the colorless polyimide LaRC-CP2 [16]. This optically transparent polyimide is resistant to radiation and may be used to make thin polymer films for building large space structures. The mechanical properties of this polymer are not known *a priori*, and have been experimentally determined as described in section 7.2.

In order to synthesize the composite nanotube/LaRC-CP2 composite, a batch of purified laser-ablated SWNTs was obtained from Rice University, and transmission electron microscope (TEM) and

atomic force microscope (AFM) observation revealed an average SWNT radius and length of approximately 0.7 nm and 3000 nm, respectively. The diamine and dianhydride used to synthesize the LaRC-CP2 were 1,3-bis(3-aminophenoxy) benzene (APB) and 2,2-bis(3,4-anhydrodicarboxyphenyl) hexafluoropropane (6FDA), respectively. As-received anhydrous dimethyl formamide (DMF) was used as a solvent. The details of the synthesis are described elsewhere [17].

A dilute SWNT solution, typically around 0.05% weight fraction in DMF, was prepared by homogenizing for 10 min (750 rpm with a 6 mm diameter rotor homogenizer) and sonicating for an hour at 47 kHz. In addition, a sample of purified SWNTs was additionally treated with an acid mixture in order to study the effect of additional SWNT treatment on the dispersion of nanotubes. The acid mixture was prepared in a round bottom flask with concentrated H_2SO_4 and HNO_3 in the ratio of 3 to 1. The purified SWNT was added into the acid mixture and refluxed at 70˚C for 30 min to make a dark brown solution. The dark solution was diluted with distilled water and allowed to settle overnight. A clear amber supernatant was decanted and the remaining dark solution containing the sediment was filtered through a sintered glass filter and washed thoroughly with distilled water and methanol under vacuum. A dried SWNT paper was peeled off from the filter and dried in a vacuum oven at 60˚C overnight. The acid-treated SWNT solution was also prepared as a dilute solution in DMF in the same manner described above. The sonicated SWNT solution was used as a solvent for the poly(amic acid) synthesis with the diamine and dianhydride. The entire reaction was carried out while stirring in a nitrogen-purged flask immersed in a 40 kHz ultrasonic bath until the solution viscosity increased and stabilized. Sonication was ceased and stirring was continued for several hours to form a SWNT-poly(amic acid) solution. Acetic anhydride and pyridine were added as catalysts with stirring to imidize the SWNT-poly(amic acid) chemically.

A series of SWNT/LaRC-CP2 nanocomposite films were prepared with a SWNT concentration of up to 1.0% nanotube weight fraction for both the as-received (which is the baseline system) and acid treated systems. The SWNT-poly(amic acid) solution prepared was cast onto a glass plate and dried in a dry air-flowing chamber. Subsequently, the dried tack-free film was cured in a nitrogen-circulating oven to obtain solvent-free freestanding SWNT-polyimide film. Examination of the films with Transmission Electron Microscopy and an optical microscope revealed that thin SWNT bundles were dispersed uniformly throughout the whole polymer matrix [17].

3. Molecular potential energy. The bonded and non-bonded interactions of the atoms in a molecular structure can be quantitatively described by using molecular mechanics. The forces that exist for each bond, as a result of the relative atomic positions, are described by the force field such that these forces contribute to the total molecular potential energy of a molecular system. The molecular potential energy for a nano-structured material is subsequently described by the sum of the individual energy contributions in the molecular model (Fig. 1). The individual energy contributions are summed over the total number of corresponding interactions in the molecular model. Various functional forms may be used for these energy terms depending on the particular material and loading conditions considered [18].

In this study, the total molecular potential energy of the molecular model is taken to be:

$$\Lambda^m = \sum_a K_a^{\rho} \left(\rho_a - \mathrm{P}_a\right)^2 + \sum_a K_a^{\theta} \left(\theta_a - \Theta_a\right)^2 + \sum_a D_a^{\mathrm{IJ}} \left[\frac{1}{2} \left(\frac{\rho_a^{\mathrm{IJ}}}{\rho_a} \right)^{12} - \left(\frac{\rho_a^{\mathrm{IJ}}}{\rho_a} \right)^{6} \right] \tag{1}$$

where the terms P_a and Θ_a refer to the undeformed interatomic distance of bond number *a* and the undeformed bond-angle number *a*, respectively. The quantities ρ_a and θ_a are the distance and bond-angle

after stretching and angle variance, respectively. The symbols K_a^{ρ} and K_a^{θ} represent the force constants associated with the stretching and angle variance of bond and bond-angle number *a*, respectively. The well depth and natural van der Waals distance for interaction *a* are given by, respectively [18]:

$$D_a^{IJ} = \sqrt{D_a^I \cdot D_a^J}$$
$$\rho_a^{IJ} = \sqrt{\rho_a^I \cdot \rho_a^J} \tag{2}$$

where the superscripts I and J denote the two atoms involved in an individual van der Waals interaction. Only the bond stretching, bond-angle variation, and van der Waals parameters were considered in Eq. (1) since other energy terms were found to have a negligible contribution to the total molecular potential energy. The values of the force constants, well depths, and natural van der Waals distances, equilibrium bond lengths, and equilibrium bond angles associated with the Carbon, Hydrogen, and Oxygen atoms shown in Fig. 2 are listed in Tables 1-3.

4. Molecular dynamics simulation. Molecular Dynamics (MD) simulation has become an effective tool for studying the physics of condensed matter systems in which the forces acting on particles in a defined cell are calculated and the classical Newtonian equations of motion are integrated numerically [19-21]. In general, each particle is allowed to interact with all the other particles in the simulation.

In the present study, a MD simulation was used to generate the equilibrium structure of the composite system, which consisted of a (6,6) single-walled nanotube and five PmPV oligomers, each ten repeating units in length. The initial structure was constructed by placing the nanotube at the center of the MD cell, and by inserting the PmPV molecules at random, non-overlapping positions within the MD cell. This sample was equilibrated for approximately 500ps at 800K and 500 atm of hydrostatic pressure to relax the initial configuration and compress the system to an appropriate density. This initial procedure was followed by an additional 500ps of simulation at 300K and 1 atm of pressure. By the end of the final equilibration run, the total energy and density had stabilized. No constraints were placed on the periodic MD cell shape or size.

The parameters used in the MD simulation are listed in Tables 1-3, with the atom labels defined in Fig. 2. All parameters, other than those involving the oxygen atom were taken from the OPLS-AA force field developed by Jorgensen and coworkers [22-24]. Parameters for the ether linkage were adapted from the MM3 force field [25-27]. All simulations were carried out with the TINKER® 3.8 [28] molecular modeling package and were performed in the constant NPT ensemble, using the Berendsen weak coupling method to maintain the temperature and pressure near their specified values [29]. A modified Beeman integration algorithm, as implemented in the Tinker 3.8 package, was used to integrate the equations of motion [30]. The resulting molecular model is shown on the left side of Fig. 3.

5. Equivalent-continuum modeling. The equivalent-continuum model of the composite material can be developed based on the equilibrium molecular structure obtained with the MD simulation by using the methods of Odegard *et al.* [6]. This approach relies on an equivalent-continuum modeling technique that is used to predict the bulk mechanical behavior of nano-structured materials. In summary, the method consists of two major steps. First, a suitable representative volume element (RVE) of the nano-structured material is chosen. The RVE of a typical nano-structured material is on the nanometer length scale, therefore, the material of the RVE is not continuous, but is an assemblage of many atoms. Interaction of these atoms is described in terms of molecular mechanics force constants, which are known for most atomic structures [18]. In the second step, an equivalent-continuum model of the RVE is

developed in which the total strain energy in the molecular and equivalent-continuum models, under identical loading conditions, is set to be equal. The effective mechanical properties, or the effective geometry, of the equivalent-continuum is then determined from equating strain energies.

For the most general approach, an equivalent-truss model of the RVE may be developed as an intermediate step to link the molecular and equivalent-continuum models. Each atom in the molecular model is represented by a pin-joint, and each truss element represents an atomic bonded or non-bonded interaction. The moduli of the truss elements are based on the molecular mechanics force constants. Therefore, the total molecular potential energy of the molecular model and the strain energy of the equivalent-truss are equal for the same loading conditions.

5.1. Truss model. In traditional molecular models, the atomic lattice has been viewed as an assemblage of discrete masses that are held in place with atomic forces that resemble elastic springs [31]. The mechanical analogy of this model is a pin-jointed truss model in which each truss member represents either a bonded or non-bonded interaction between atoms. Therefore, the truss model allows the mechanical behavior of the nano-structured system to be accurately modeled in terms of displacements of the atoms. The deformation of each bonded or non-bonded interaction corresponds to the axial deformation of the corresponding truss element.

The total mechanical strain energy, Λ^t, of the truss model is:

$$\Lambda^{\mathrm{t}} = \sum_b \sum_a \frac{A_a^b E_a^b}{2R_a^b}\left(r_a^b - R_a^b\right)^2 \tag{3}$$

where A_a^b and E_a^b are the cross-sectional area and Young's modulus of rod *a* of truss member type *b*, respectively. The term $r_a^b - R_a^b$ is the stretching of rod *a* of truss member type *b*, where R_a^b and r_a^b are the undeformed and deformed lengths of the truss elements, respectively.

In order to represent the mechanical behavior of the molecular lattice model with the truss model, Eq. (3) must be equated with Eq. (1) in a physically meaningful manner. Both equations are the sum of energies for particular degrees of freedom. The main difficulty in the substitution is specifying Eq. (3), which has stretching terms only, for Eq. (1), which also has bond-angle variance and van der Waals terms.

It was shown by Odegard *et al.* [6] that for small deformations, the Young's moduli of the rods representing primary bonds and the bond-angle variance interactions may be determined as a function of the force constants:

$$E_a^{\alpha} = \frac{2K_a^{\rho}R_a^{\alpha}}{A_a^{\alpha}} \tag{4}$$

$$E_a^{\beta} = \frac{32K_a^{\theta}}{A_a^{\beta}R_a^{\beta}}\left(\sin\frac{\Theta_a}{2}\right)^2 \tag{5}$$

where K_a^{ρ}, K_a^{θ}, and Θ_a are the same parameters associated with Eq. (1), and the superscripts α and β indicate primary bonding and bond-angle variance interactions, respectively.

Upon examination of Eq. (1), it is clear that the energy associated with van der Waals interactions is highly non-linear with respect to interatomic distance. The determination of the Young's moduli of truss

elements that represent van der Waals interactions is complicated by accounting for this non-linearity and the large range of values for the interatomic distance of the interacting atoms in an equilibrium configuration. Therefore, linear relationships for the Young's modulus, such as those given by Eqs. (4) and (5), are not realistic for the van der Waals interactions.

To address this problem, the energy associated with the van der Waals interaction given in Eq. (1) and the strain energy of a truss element given by Eq. (3) were equated. The Young's modulus that represents the mechanical stiffness of a van der Waals interaction is given by:

$$E_a^{\omega} = \frac{2\rho_a^{IJ} D_a^{IJ}}{A_a^{\delta}\left(\rho_a - \rho_a^{IJ}\right)^2}\left[\frac{1}{2}\left(\frac{\rho_a^{IJ}}{\rho_a}\right)^{12} - \left(\frac{\rho_a^{IJ}}{\rho_a}\right)^{6}\right] \tag{6}$$

where the superscript ω indicates van der Waals bonding. Clearly, the Young's modulus is highly dependent on the interatomic spacing. However, because of the difficulty of assigning an individual Young's modulus value for every van der Waals interaction in a nano-structured material, discrete values of Young's modulus may be approximated for ranges of interatomic spacing for each combination of atoms based on Eq. (6). The process for establishing these ranges is discussed below.

To implement the resultant equivalent-truss structure, a finite element model was developed by using ANSYS® 6 [32] (Fig. 3). Each element (LINK8) was a three-dimensional pin-jointed truss element with six degrees of freedom (three displacement components on each end) that represented a single atomic interaction. Each node corresponded to an atom in the equilibrium structure of the molecular model. A total of 14,501 elements and 1,818 nodes were used in the model.

5.2. Continuum model. With the equivalent-truss structure in place, the continuum model could be constructed. The geometry of the linear-elastic, homogeneous, equivalent-continuum RVE was assumed to be cylindrical, similar to that of the molecular and truss models (Fig. 3). With this approach, the mechanical properties of the solid cylinder were determined by equating the total strain energies of the equivalent-truss and equivalent-continuum models under identical loading conditions. Examination of the molecular model revealed that it was accurately described as having transversely isotropic symmetry, with the plane of isotropy perpendicular to the long axis of the nanotube. There are five independent material parameters required to determine the entire set of elastic constants for a transversely isotropic material. Each of the five independent parameters may be determined from a single boundary condition applied to both equivalent-truss and equivalent-continuum models. Once the mechanical properties of the equivalent-continuum RVE are determined, then the model may be used in subsequent micromechanical analyses as an effective fiber. The method employed in this study was adapted from the approach used by Hashin and Rosen [33] to determine elastic properties for fiber reinforced composite materials.

5.2.1. Effective fiber constitutive model. The constitutive relationship of the transversely isotropic equivalent-continuum RVE (which is referred to as the effective fiber throughout the remainder of the paper) is:

$$\sigma_{ij} = C_{ijkl}^{f} \varepsilon_{kl} \tag{7}$$

where σ_{ij} and ε_{kl} are the stress and strain components, respectively (i,j = 1,2,3), and C^f_{ijkl} are the elastic stiffness components of the effective fiber (denoted by superscript *f*). Alternatively, Eq. (7) can be simplified by using the usual contracted notation for the elastic stiffness components and transversely-isotropic symmetry:

$$
\begin{aligned}
\sigma_{11} &= C^f_{11}\varepsilon_{11} + C^f_{12}\varepsilon_{22} + C^f_{12}\varepsilon_{33} \\
\sigma_{22} &= C^f_{12}\varepsilon_{11} + C^f_{22}\varepsilon_{22} + C^f_{23}\varepsilon_{33} \\
\sigma_{33} &= C^f_{12}\varepsilon_{11} + C^f_{23}\varepsilon_{22} + C^f_{22}\varepsilon_{33} \\
\sigma_{12} &= 2C^f_{44}\varepsilon_{12} \\
\sigma_{13} &= 2C^f_{44}\varepsilon_{13} \\
\sigma_{23} &= \left(C^f_{22} - C^f_{23}\right)\varepsilon_{23}
\end{aligned}
\tag{8}
$$

Five independent elastic properties may be chosen to describe the complete set of elastic stiffness components, namely, the elastic stiffness component, C^f_{11}, and four elastic parameters: transverse shear modulus, G^f_T, transverse bulk modulus (also known as the plane-strain bulk modulus), K^f_T, longitudinal shear modulus, G^f_L, and longitudinal Young's modulus, E^f_L. The four elastic parameters are related to the elastic stiffness components by:

$$
\begin{aligned}
G^f_T &= \frac{1}{2}\left(C^f_{22} - C^f_{23}\right) \\
K^f_T &= \frac{1}{2}\left(C^f_{22} + C^f_{23}\right) \\
G^f_L &= C^f_{44} \\
E^f_L &= C^f_{11} - \frac{2C^{f\,2}_{12}}{C^f_{22} + C^f_{23}}
\end{aligned}
\tag{9}
$$

Conversely, the elastic stiffness components can be described in terms of the four elastic parameters:

$$
\begin{aligned}
C^f_{44} &= G^f_L \\
C^f_{22} &= G^f_T + K^f_T \\
C^f_{23} &= K^f_T - G^f_T \\
C^f_{12} &= \left[K^f_T\left(C^f_{11} - E^f_L\right)\right]^{\frac{1}{2}}
\end{aligned}
\tag{10}
$$

At this point, both the elastic parameters and the elastic stiffness components are unknown. These values are determined by applying five identical sets of boundary conditions to the equivalent-truss model and the effective fiber, and by subsequently equating the strain energies by adjusting the five independent elastic properties. Boundary conditions must be chosen to yield unique values for the independent elastic properties.

5.2.2. Boundary conditions. Five sets of boundary conditions were chosen to determine each of the five independent elastic properties such that a single property could be independently determined for each boundary condition. The displacements and tractions applied at the boundaries of the RVE are generalized, respectively, by:

$$u_i(B) = \varepsilon_{ij} x_j \tag{11}$$

$$T_i(B) = \sigma_{ij} n_j \tag{12}$$

where B is the bounding surface, x_j is defined in Fig. 3, and n_j are the components of the outward normal to B. The generalized total strain energy of the effective fiber is:

$$\Lambda^f = \frac{V}{2}\sigma_{ij}\varepsilon_{ij} = \frac{\pi D^2 L}{8}\sigma_{ij}\varepsilon_{ij} \tag{13}$$

where V, D, and L are the volume, diameter, and length of the effective fiber, respectively (Fig. 3). The boundary conditions and strain energies for each of the five independent elastic properties are described below.

5.2.2.1. Transverse shear modulus. For a pure transverse shear strain, e, applied to the boundary of the equivalent-truss RVE and the effective fiber, we have $\varepsilon_{23} = e/2$, with the remaining strain components equal to zero. From Eq. (11) the boundary displacements are:

$$\begin{aligned} u_1(B) &= 0 \\ u_2(B) &= \frac{e}{2} x_3 \\ u_3(B) &= \frac{e}{2} x_2 \end{aligned} \tag{14}$$

From Eq. (13) the total strain energy of the effective fiber is:

$$\Lambda^f = \frac{1}{8}\pi D^2 L G_T^f e^2 \tag{15}$$

where D and L are the diameter and length of the effective fiber, respectively (Figure 3). The effective fiber strain energy, Λ^f, is equated to the strain energy of the truss subjected to the boundary conditions in Eq. (14). Since D and L are known, and e is arbitrarily chosen in determining Λ^f (in the range of small deformations, i.e. $e \ll 1$), then the transverse shear modulus of the effective fiber is directly evaluated from Eq. (15).

5.2.2.2. Transverse bulk modulus. The transverse bulk modulus was obtained in a similar manner by prescribing transverse strains $\varepsilon_{22} = \varepsilon_{33} = e$ to the RVE boundary with all remaining strain components set to zero. From Eq. (11) the displacements are:

$$\begin{aligned} u_1(B) &= 0 \\ u_2(B) &= ex_2 \\ u_3(B) &= ex_3 \end{aligned} \tag{16}$$

The strain energy of the effective fiber for this case is:

$$\Lambda^f = \frac{1}{2}\pi D^2 L K_T^f e^2 \tag{17}$$

The transverse bulk modulus was determined from Eq. (17).

5.2.2.3. Longitudinal shear modulus. The longitudinal shear modulus was determined by prescribing a pure shear strain in the 1-2 plane, $\varepsilon_{12} = e/2$, with the remaining strain components set equal to zero. Therefore, the applied boundary displacements are:

$$\begin{aligned} u_1(B) &= \frac{e}{2}x_2 \\ u_2(B) &= \frac{e}{2}x_1 \\ u_3(B) &= 0 \end{aligned} \tag{18}$$

The resulting strain energy of the effective fiber is:

$$\Lambda^f = \frac{1}{8}\pi D^2 L G_L^f e^2 \tag{19}$$

The longitudinal shear modulus was evaluated using Eq. (19).

5.2.2.4. Longitudinal Young's modulus. The longitudinal Young's modulus was determined by prescribing a strain along the 1-axis, $\varepsilon_{11} = e$, with all of the shear strain components set to zero. Since a transverse Poisson contraction is allowed in this case, the transverse normal stresses are set to zero, $\sigma_{22} = \sigma_{33} = 0$. From Eqs. (11) and (12), the boundary conditions are:

$$u_1(B) = ex_1$$
$$T_2(B) = 0 \tag{20}$$
$$T_3(B) = 0$$

The strain energy is:

$$\Lambda^f = \frac{1}{8}\pi D^2 L E_L^f e^2 \tag{21}$$

The longitudinal Young's modulus was evaluated using Eq. (21).

5.2.2.5. Elastic stiffness component C_{11}^f. The elastic stiffness tensor component, C_{11}^f, may be determined by applying a strain parallel to the 1-axis, while constraining the strains along the 2- and 3-axes, therefore preventing a Poisson contraction. For a prescribed strain, $\varepsilon_{11} = e$, with the remaining strains held at zero, the displacements from Eq. (11) are:

$$u_1(B) = ex_1$$
$$u_2(B) = 0 \tag{22}$$
$$u_3(B) = 0$$

From Eq. (13), the strain energy for these displacements is:

$$\Lambda^f = \frac{1}{8}\pi D^2 L C_{11}^f e^2 \tag{23}$$

Therefore, the elastic stiffness component C_{11}^f can be used as one of the five independent parameters that describe the overall properties of the transversely isotropic effective fiber.

5.2.3. Boundary region. The displacements and tractions specified above were applied to each node in the boundary region of the equivalent-truss model (indicated in Fig. 3), and the corresponding strain energies were calculated by summing the strain energies of each individual truss member in the RVE.

To determine the size of the boundary region, it was assumed that the range of the boundary region is related to the interatomic distance between the minimum non-bonded spacing found in the equilibrium structure to the maximum distance for which a positive-definite relationship exists between the force and displacement. It was also assumed that the contribution of the energies associated with van der Waals forces between atoms with a separation distance larger than this maximum were relatively small and could be neglected.

The recent MD simulation of a SWNT surrounded by polyethylene molecules performed by Wise and Hinkley [5] predicted that the local changes in the polymer molecular structure and the non-functionalized SWNT/polymer interface are on the same length scale as the width of the nanotube. This recent study and the aforementioned assumptions led to the selection of a cylindrical boundary region that

extends to a radius of 0.9 nm measured from the center of the nanotube to the outer edge of the molecular model (Fig. 3). Within the 0.9 nm radius, the RVE includes the nanotube, nanotube/polymer interface, and polymer molecules immediately adjacent to the interface.

5.2.4. Material property summary. For an effective fiber diameter, D, of 1.8 nm, length, L, of 3.2 nm, and applied strain, e, of 0.1%, the calculated values of the five independent parameters and the resulting elastic stiffness tensor components for the effective fiber calculated from Eq. (10) are listed in Table 4.

6. Micromechanical analysis. The effective fiber accurately accounts for the structure-property relationships at the nanoscale and provides a bridge to the continuum model. With this process firmly established, constitutive models of the effective fiber/polymer composite may be developed with a micromechanical analysis by using the mechanical properties of the effective fiber and the bulk polymer matrix material. For the composite considered in this study, the PmPV molecules that were near the polymer/nanotube interface were included in the effective fiber, and it was assumed that the matrix polymer surrounding the effective fiber had mechanical properties equal to those of the bulk LaRC-SI and LaRC-CP2 resin. Because the bulk polymer molecules and the polymer molecules included in the effective fiber are physically entangled, perfect bonding between the effective fiber and the surrounding polymer matrix was assumed.

To address scale-up, the micromechanics-based Mori-Tanaka method [34] was used to predict the elastic stiffness properties of the effective fiber-polymer composite material. This method has been successfully applied to transversely-isotropic inclusions by Qui and Weng [35] and for this current method, the complete elastic stiffness tensor for the composite is given by Benveniste [36]

$$\mathbf{C} = \mathbf{C}^m + v_f \left\langle \left(\mathbf{C}^f - \mathbf{C}^m \right) \mathbf{A}^f \right\rangle \left(v_m \mathbf{I} + v_f \left\langle \mathbf{A}^f \right\rangle \right)^{-1} \tag{24}$$

where v_f and v_m are the fiber and matrix volume fractions, respectively, $\mathbf{I}$ is the identity tensor, $\mathbf{C}^m$ is the stiffness tensor of the matrix material, $\mathbf{C}^f$ is the stiffness tensor of the fiber, and $\mathbf{A}^f$ is the dilute mechanical strain concentration tensor for the fiber

$$\mathbf{A}^f = \left[\mathbf{I} + \mathbf{S}\mathbf{C}^{m^{-1}} \left(\mathbf{C}^f - \mathbf{C}^m \right) \right]^{-1} \tag{25}$$

The tensor $\mathbf{S}$ is Eshelby's tensor as given by Eshelby [37] and Mura [38]. The terms enclosed with angle-brackets in Eq. (24) represent the average value of the term over all orientations defined by transformation from the local fiber coordinates (x_1, x_2, x_3) to the global coordinates (x_1''', x_2''', x_3''') (Fig. 4). For example, the transformed dilute mechanical strain concentration tensor for the fiber with respect to the global coordinates is

$$\overline{\mathrm{A}}^f_{ijkl} = c_{ip} c_{jq} c_{kr} c_{ls} \mathrm{A}^f_{pqrs} \tag{26}$$

where c_{ij} are the direction cosines for the transformation indicated in Fig. 4; that is,

$$
\begin{aligned}
c_{11} &= \cos\phi\cos\psi - \sin\phi\cos\gamma\sin\psi \\
c_{12} &= \sin\phi\cos\psi + \cos\phi\cos\gamma\sin\psi \\
c_{13} &= \sin\psi\sin\gamma \\
c_{21} &= -\cos\phi\sin\psi - \sin\phi\cos\gamma\cos\psi \\
c_{22} &= -\sin\phi\sin\psi + \cos\phi\cos\gamma\cos\psi \\
c_{23} &= \sin\gamma\cos\psi \\
c_{31} &= \sin\phi\sin\gamma \\
c_{32} &= -\cos\phi\sin\gamma \\
c_{33} &= \cos\gamma
\end{aligned}
\tag{27}
$$

In general, the orientation average of the dilute mechanical strain concentration tensor is [39]

$$
\left\langle \mathbf{A}^f \right\rangle = \frac{\int_{-\pi}^{\pi}\int_{0}^{\pi}\int_{0}^{\pi/2} \overline{\mathrm{A}}^f\left(\phi,\gamma,\psi\right)\lambda\left(\phi,\psi\right)\sin\left(\gamma\right)\mathrm{d}\phi\mathrm{d}\gamma\mathrm{d}\psi}{\int_{-\pi}^{\pi}\int_{0}^{\pi}\int_{0}^{\pi/2} \lambda\left(\phi,\psi\right)\sin\left(\gamma\right)\mathrm{d}\phi\mathrm{d}\gamma\mathrm{d}\psi}
\tag{28}
$$

where $\lambda\left(\phi,\psi\right)$ is the orientation distribution function

$$
\lambda\left(\phi,\psi\right) = \exp\left[-s_1\phi^2\right]\exp\left[-s_2\psi^2\right]
\tag{29}
$$

and where s_1 and s_2 are factors that control the orientation. Three cases considered in this paper are

$$
\begin{aligned}
&\text{random}: s_1 = 0, s_2 = 0 && \lambda\left(\phi,\psi\right) = 1 \\
&\text{aligned}: s_1 = \infty, s_2 = \infty && \lambda\left(\phi,\psi\right) = \delta\left(\phi - 0\right)\delta\left(\psi - 0\right) \\
&\text{axisymmetric}: s_1 = k, s_2 = \infty && \lambda\left(\phi,\psi\right) = \exp\left[-k\phi^2\right]\delta\left(\psi - 0\right)
\end{aligned}
\tag{30}
$$

where $\delta\left(y - \overline{y}\right)$ is Dirac's delta distribution, centered at $\overline{y}$. The random case is a completely three dimensionally randomly oriented composite. The aligned case corresponds to fibers perfectly aligned along the $x_1^{'''}$ axis. The axisymmetric case is an axisymmetric distribution of fibers about the $x_1^{'''}$ axis. The constant k describes the relative amount of alignment of the fibers with respect to the $x_1^{'''}$ axis. For large values of k ($k \to \infty$), the axisymmetric distribution approaches the aligned case, and for small values of k ($k \to 0$), the fibers are axisymmetrically distributed over all values of the angle ϕ with respect to the $x_1^{'''}$ axis. A plot of the orientation distribution functions for various intermediate values of k is shown in Fig. 5.

For the effective fiber/polymer composites considered in this study, the elastic stiffness components, volume fraction, length, and orientation of the effective fiber were used for the fiber properties in Eqs. (24) and (25). The effective fibers were assumed to have a spheroid geometry for the Eshelby tensor in Eq. (25). The triple integral in Eq. (28) was numerically evaluated using the extended trapezoidal rule [40].

7. Results.

7.1. SWNT/LaRC-SI composite. In this section, the moduli of the effective fiber/polymer composite are presented in terms of nanotube length, volume fraction, and orientation distribution. While the nanotube and effective fiber lengths are equal, the nanotube volume fraction was determined to be 34% of the effective fiber volume fraction if it is assumed that the nanotube volume is a hollow cylinder with a wall thickness equal to interatomic spacing of graphene sheets (0.34 nm). The properties of the composite with randomly and axisymmetrically oriented nanotubes were calculated for nanotube lengths up to 200 nm. This maximum length was chosen based on the decreased likelihood of a typical nanotube remaining straight as the nanotube length exceeds 200 nm.

Fig. 6 is a plot of the calculated longitudinal Young's modulus, E_L, and longitudinal shear modulus, G_L, for the random, aligned, and axisymmetric composites as a function of nanotube length, for a 1% nanotube volume fraction. These quantities were calculated from the elastic stiffness tensor of the composite, **C**, using equation for the composite. The results indicate that there is an approximately 55% increase in the shear modulus of the randomly oriented nanotube composite in the range of nanotube lengths between 0 to 200 nm, with a significant change in the slope occurring between nanotube lengths of 50 and 100 nm. Conversely, the calculated longitudinal shear modulus for the aligned nanotube composite was constant for the given range of nanotube length. Therefore, under these conditions, increasing the degree of alignment resulted in a decrease in shear modulus.

From Fig. 6 it can be seen that there is about a 400% increase in the longitudinal Young's modulus for the aligned composite with 200 nm long nanotubes with respect to the polymer system without reinforcement. The data also indicate that alignment of the nanotubes results in nearly a 300% increase in the longitudinal Young's modulus for the composite with nanotubes that are 200 nm long. Unlike the case for shear modulus, an increase in the degree of alignment resulted in an increase in the longitudinal Young's modulus. A significant decrease in the slope of the Young's modulus curves occurs between nanotube lengths of 60 to 80 nm.

The longitudinal Young's modulus of the aligned composite is plotted in Fig. 7 as a function of nanotube volume fraction for 10, 50, and 500 nm long nanotubes. Young's modulus increases with an increase in volume fraction, with the most pronounced rate of increase associated with nanotubes of length 50 nm or greater. The dependence of the longitudinal Young's modulus on the nanotube volume fraction becomes more linear as the nanotube length increases. This is expected due to the well-known effect of the increase in load transfer with subsequent increases in reinforcement length and volume fraction [41]. For 500 nm long aligned nanotubes, the longitudinal Young's modulus of a 25% nanotube volume fraction composite is about 85 times larger than the Young's modulus of the un-reinforced resin.

Fig. 8 is a plot of the Young's modulus and the shear modulus for the random composite as a function of nanotube volume fraction, for three nanotube lengths. In general, an increase in nanotube volume fraction results in increased moduli values. For both the Young's and the shear moduli, increasing the volume fraction for the short nanotubes of length near 10 nm provides little to no improvement in stiffness. However, for nanotubes between 50 nm to 200 nm, equivalent stiffness can easily be obtained by trading off a decrease in nanotube length for a small (2x or less) change in volume fraction. Increasing the nanotube length above 200 nm results in negligible increases in modulus.

The longitudinal Young's modulus for the axisymmetric composite is plotted in Fig. 9 as a function of nanotube volume fraction for 200 nm long nanotubes. Three different values of k are shown. For comparison, the plots for a random and aligned composite are also shown for 200 nm long nanotubes. It is clear that the variation of the alignment factor k has a significant effect on the Young's modulus. As k

increases and decreases, the longitudinal Young's modulus of the axisymmetric composite approaches that of the aligned composite and random composite, respectively.

7.2. SWNT/LaRC-CP2 composite. In this section, the Young's modulus of the SWNT/LaRC-CP2 composite is determined as a function of nanotube volume fraction, and compared to experimentally determined values of Young's modulus. Mechanical properties of the films were evaluated by a Rheometrics dynamic mechanical analyzer (DMA). The film specimens had dimensions of 12 mm × 5mm × 35 μm, and were dynamically loaded in tension at a constant frequency of 1 Hz. A plot of the experimental data is shown in Fig. 10 for the composite material prepared with both the as-received and acid-treated nanotubes. It is assumed that the Young's modulus is equal to the storage modulus obtained from the DMA at room temperature. Even though a total of three tests were performed for each data point, only one set of the data points is shown in Fig. 10 since the replicate values were nearly identical with the set shown. The conversion of nanotube weight fraction to nanotube volume fraction was performed using the methodology of Pipes *et al.* [42]. It was assumed that the volume of the nanotube is defined as a solid cylinder with a radius equal to the sum of radius of the nanotube carbon atoms and half of the distance between the nanotube carbon atoms and the radius of the closest polymer atoms. It can be seen from Fig. 10 that the Young's modulus of the composite with acid-treated nanotubes is slightly larger than the composite with the as-received nanotubes.

The effective fiber properties determined in section 7.1 were used to model the SWNT/LaRC-CP2 composite. The Young's modulus of the LaRC-CP2 neat resin was taken from the experimental data for a 0% nanotube volume fraction (0.85 GPa), and a typical value of Poisson's ratio for a polyimide was assumed (0.4). It was determined that the nanotube volume fraction was 37% of the effective fiber volume fraction if it is assumed that the nanotube volume is defined as stated above for the conversion of nanotube weight fraction to volume fraction. The properties of the composite material with randomly oriented nanotubes were calculated for nanotube lengths of 3000 nm. The predicted Young's modulus as a function of nanotube volume fraction is shown in Fig. 10. Even though there is good agreement between the model and the acid-treated nanotube composite, the predicted values of modulus are larger than the measured values for the as-received material, especially for values of nanotube volume fraction greater than about 0.5%. For example, at 0.21% nanotube volume fraction, the predicted Young's modulus is 12% and 35% higher than the measured values from the acid-treated and as-received materials, respectively. The difference between the experiments and the model is most likely due to the fact that while the model assumes that the effective fibers are perfectly dispersed in the polymer matrix, a significant amount of nanotubes remain in bundles in the composite material, as shown by Park *et al.* [17]. The closer agreement between the model and the acid-treated values indicates that the nanotubes are more dispersed in the acid-treated material than in the as-received material.

8. Summary and conclusions. In this study, a method has been presented for linking atomistic simulations of nano-structured materials to continuum models of the corresponding bulk material. For a polymer composite system reinforced with single-walled carbon nanotubes (SWNT), the method provides the steps whereby the nanotube, the local polymer near the nanotube, and the nanotube/polymer interface can be modeled as an effective continuum fiber by using an equivalent-continuum model. The effective fiber retains the local molecular structure and bonding information, as defined by molecular dynamics, and serves as a means for linking the equivalent-continuum and micromechanics models. The micromechanics method is then available for the prediction of bulk mechanical properties of SWNT/polymer composites as a function of nanotube size, orientation, and volume fraction. The utility of this method was examined by modeling SWNT/LaRC-SI and SWNT/LaRC-CP2 composites, both having a PmPV interface. The elastic stiffness

constants of the SWNT/LaRC-SI composite were determined for both aligned and three-dimensional randomly oriented nanotubes, as a function of nanotube length and volume fraction. The Young's modulus of the SWNT/LaRC-CP2 composite was determined for the three-dimensionally randomly oriented nanotubes as a function of nanotube volume fraction.

For the SWNT/LaRC-SI composite at 1% nanotube volume fraction, stiffness will approach a maximum for nanotube lengths of 60 to 80 nm or greater for aligned, axisymmetric, and random nanotube orientations. Lengths above this range will also provide the most efficient increase in modulus for small changes in nanotube volume fraction. As length increases above this range, there is a limiting value such that small gains are realized for lengths above approximately 200 nm. This limiting value indicates that for nanotube lengths of approximately 200 nm, the efficiency of load transfer is nearly maximized. For long nanotubes (at least 200 nm), the relationship between stiffness and volume fraction is linear, which resembles the usual rule-of-mixtures approximation for long-fiber composites. For short, aligned nanotubes (10 nm), the volume fraction must exceed 10% before stiffness gains can be obtained. For randomly oriented nanotubes, measurable stiffness gains can be realized for small volume fractions.

For the SWNT/LaRC-CP2 composite with three-dimensionally randomly-oriented fibers, the Young's modulus is predicted to increase significantly for small volume fractions. Comparison with experiments suggests that these stiffness gains can only be achieved when the nanotubes no longer remain in their bundled form. The composite with the acid-treated nanotubes demonstrates a closer agreement with the model than the composite with the as-received nanotubes.

For many nano-structured materials, the trade-offs between structure and property must be established before the material can be optimized for any given application. The method presented in this paper provides a means for parametrically exploring these structure-property relationships. The method is applicable to a wide range of problems that require the accuracy of atomistic level descriptions coupled with the general applicability of continuum-level models.

Acknowledgements. This work was partially performed while Dr. Odegard and Dr. Wise held National Research Council Research Associateship Awards at NASA Langley Research Center.

References

[1] R.L. MCCULLOUGH, *Micro-Models for Composite Materials - Continuous Fiber Composites*, in J.M. Whitney, and R.L. McCullough, eds., *Delaware Composites Design Encyclopedia-Volume 2: Micromechanical Materials Modeling*, Technomic Pub. Co., Lancaster, PA, 1990, pp. 49-90.

[2] R.L. MCCULLOUGH, *Micro-Models for Composite Materials - Particulate and Discontinuous Fiber Composites*, in J.M. Whitney, and R.L. McCullough, eds., *Delaware Composites Design Encyclopedia-Volume 2: Micromechanical Materials Modeling*, Technomic Pub. Co., Lancaster, PA, 1990, pp. 93-142.

[3] D. QIAN, E.C. DICKEY, R. ANDREWS, and T. RANTELL, *Load Transfer and Deformation Mechanisms in Carbon Nanotube-Polystyrene Composites*, Applied Physics Letters, 76 (2000), pp. 2868-2870.

[4] M.S.P. SHAFFER, and A.H. WINDLE, *Fabrication and Characterization of Carbon Nanotube/Poly(vinyl alcohol) Composites*, Advanced Materials, 11 (1999), pp. 937-941.

[5] K. WISE, and J. HINKLEY, *Molecular Dynamics Simulations of Nanotube-Polymer Composites*, *American Physical Society Spring Meeting, April 12-16, 2001*, Seattle, WA, 2001.

[6] G.M. ODEGARD, T.S. GATES, L.M. NICHOLSON, and K. WISE, *Equivalent-Continuum Modeling With Application to Carbon Nanotubes*, NASA/TM-2002-211454, 2002.

[7] S. IIJIMA, *Helical Microtubules of Graphitic Carbon*, Nature, 354 (1991), pp. 56-58.

[8] A.S. EDELSTEIN, and R.C. CAMMARATA, *Nanomaterials: Synthesis, Properties and Applications*, Institute of Physics Publishing, Bristol, 1996.

[9] S.J.V. FRANKLAND, A. CAGLAR, D.W. BRENNER, and M. GRIEBEL, *Reinforcement Mechanisms in Polymer Nanotube Composites: Simulated Non-Bonded and Cross-Linked Systems*, *MRS Fall Meeting*, Boston, MA, 2000.

[10] R.J. CHEN, Y. ZHANG, D. WANG, and H. DAI, *Noncovalent Sidewall Functionalization of Single-Walled Carbon Nanotubes for Protein Immobilization*, Journal of the American Chemical Society, 123 (2001), pp. 3838-3839.

[11] A. STAR, J.F. STODDART, D. STEUERMAN, M. DIEHL, A. BOUKAI, E.W. WONG, X. YANG, S. CHUNG, H. CHOI, and J.R. HEATH, *Preparation and Properties of Polymer-Wrapped Single-Walled Carbon Nanotubes*, Angewandte Chemie International Edition in English, 40 (2001), pp. 1721-1725.

[12] L.M. NICHOLSON, K.S. WHITLEY, T.S. GATES, and J.A. HINKLEY, *Influence of Molecular Weight on the Mechanical Performance of a Thermoplastic Glassy Polyimide*, Journal of Materials Science, 35 (2000), pp. 6111-6122.

[13] L.M. NICHOLSON, K.S. WHITLEY, and T.S. GATES, *The Combined Influence of Molecular Weight and Temperature on the Physical Aging and Creep Compliance of a Glassy Thermoplastic Polyimide*, Mechanics of Time-Dependent Materials, 5 (2001), pp. 199-227.

[14] L.M. NICHOLSON, K.S. WHITLEY, and T.S. GATES, *The Role of Molecular Weight and Temperature on the Elastic and Viscoelastic Properties of a Glassy Thermoplastic Polyimide*, NASA/TM-2001-210664, 2001.

[15] K.S. WHITLEY, T.S. GATES, J. HINKLEY, and L.M. NICHOLSON, *Mechanical Properties of LaRC™ SI Polymer for a Range of Molecular Weights*, NASA/TM-2000-210304, 2000.

[16] A.K. ST. CLAIR, T.L. ST. CLAIR, and W.S. SLEMP, *Optically transparent/Colorless Polyimides*, in W. Weber, and M. Gupta, eds., *Recent Advances in Polyimide Science and Technology: Characterization and Applications*, Society of Plastics Engineers, Poughkeepsie, NY, 1987, pp. 16-36.

[17] C. PARK, Z. OUNAIES, K.A. WATSON, R.E. CROOKS, S.E. LOWTHER, J.W. CONNELL, E.J. SIOCHI, J.S. HARRISON, and T.L. ST. CLAIR, *Dispersion of Single Wall Carbon Nanotubes by In Situ Polymerization Under Sonication*, Chemical Physics Letters, in press.

[18] A.K. RAPPE, and C.J. CASEWIT, *Molecular Mechanics Across Chemistry*, University Science Books, Sausalito, California, 1997.

[19] M.P. ALLEN, and D.J. TILDESLEY, *Computer Simulation of Liquids*, Oxford University Press, Oxford, 1987.

[20] D.C. RAPAPORT, *The Art of Molecular Dynamics Simulation*, Cambridge University Press, Cambridge, 1995.

[21] D. FRANKEL, and B. SMIT, *Understanding Molecular Simulation: From Algorithms to Applications*, Academic Press, San Diego, 1996.

[22] E.M. DUFFY, P.J. KOWALCZYK, and W.L. JORGENSEN, *Do Denaturants Interact with Aromatic Hydrocarbons in Water?*, Journal of the American Chemical Society, 115 (1993), pp. 9271-9275.

[23] W.L. JORGENSEN, J.D. MADURA, and C.J. SWENSON, *Optimized Intermolecular Potential Functions for Liquid Hydrocarbons*, Journal of the American Chemical Society, 106 (1984), pp. 6638-6646.

[24] W.L. JORGENSEN, and D.L. SEVERANCE, *Aromatic-Aromatic Interactions: Free Energy Profiles for the Benzene Dimer in Water, Chloroform, and Liquid Benzene*, Journal of the American Chemical Society, 112 (1990), pp. 4768-4774.

[25] N.L. ALLINGER, Y.H. YUH, and J.H. LII, *Molecular Mechanics. The MM3 Force Field for Hydrocarbons*, Journal of the American Chemical Society, 111 (1989), pp. 8551-8566.

[26] J.H. LII, and N.L. ALLINGER, *Molecular Mechanics. The MM3 Force Field for Hydrocarbons. 2. Vibrational Frequencies and Thermodynamics*, Journal of the American Chemical Society, 111 (1989), pp. 8566-8575.

[27] J.H. LII, and N.L. ALLINGER, *Molecular Mechanics. The MM3 Force Field for Hydrocarbons. 3. The van der Waals' Potentials and Crystal Data for Aliphatic and Aromatic Hydrocarbons*, Journal of the American Chemical Society, 111 (1989), pp. 8576-8582.

[28] J.W. PONDER, *TINKER: Software Tools for Molecular Design*, Washington University School of Medicine, 1998.

[29] H.J.C. BERENDSEN, J.P.M. POSTMA, W.F. VAN GUNSTEREN, A. DINOLA, and J.R. HAAK, *Molecular Dynamics with Coupling to an External Bath*, Journal of Chemical Physics, 81 (1984), pp. 3684-3690.

[30] J.W. PONDER, *TINKER: Software Tools for Molecular Design*, Washington University School of Medicine, 2000.

[31] M. BORN, and K. HUANG, *Dynamical Theory of Crystal Lattices*, Oxford University Press, London, 1954.

[32] Anonymous, *ANSYS*, SAS IP, Canonsburg, PA, 2001.

[33] Z. HASHIN, and B.W. ROSEN, *The Elastic Moduli of Fiber-Reinforced Materials*, Journal of Applied Mechanics, 31 (1964), pp. 223-232.
[34] T. MORI, and K. TANAKA, *Average Stress in Matrix and Average Elastic Energy of Materials with Misfitting Inclusions*, Acta Metallurgica, 21 (1973), pp. 571-574.
[35] Y.P. QUI, and G.J. WENG, *On the Application of Mori-Tanaka's Theory Involving Transversely Isotropic Spheroidal Inclusions*, International Journal of Engineering Science, 28 (1990), pp. 1121-1137.
[36] Y. BENVENISTE, *A New Approach to the Application of Mori-Tanaka's Theory in Composite Materials*, Mechanics of Materials, 6 (1987), pp. 147-157.
[37] J.D. ESHELBY, *The Determination of the Elastic Field of an Ellipsoidal Inclusion, and Related Problems*, Proceedings of the Royal Society of London, Series A, A241 (1957), pp. 376-396.
[38] T. MURA, *Micromechanics of Defects in Solids*, Martinus Nijhoff, The Hague, 1982.
[39] N. MARZARI, and M. FERRARI, *Textural and Micromorphological Effects on the Overall Elastic Response of Macroscopically Anisotripic Composites*, Journal of Applied Mechanics, 59 (1992), pp. 269-275.
[40] W.H. PRESS, B.P. FLANNERY, S.A. TEUKOLSKY, and W.T. VETTERLING, *Numerical Recipes*, Cambridge University Press, Cambridge, 1986.
[41] H. FUKUDA, and Y. TAKAO, *Thermoelastic Properties of Discontinuous Fiber Composites*, in T.W. Chou, ed., *Comprehensive Composite Materials Volume 1: Fiber Reinforcements and General Theory of Composites*, Elsevier, New York, 2000, pp. 377-401.
[42] R.B. PIPES, S.J.V. FRANKLAND, P. HUBERT, and E. SAETHER, *Self-Consistent Geometry, Density and Stiffness for the SWCN and Its Hexagonal Arrays*, submitted as an ICASE report, 2002.

TABLE 1
Bond stretching parameters

Bond stretching	P (Å)	K^{ρ} (kcal/mole/ Å^2)
$C_t - C_t$	1.529	268.0
$C_t - H_t$	1.090	340.0
$C_t - O$	1.415	201.4
$C_a - O$	1.355	431.6
$C_a - C_a$	1.400	469.0
$C_a - H_a$	1.080	367.0
$C_a - C_v$	1.320	520.0
$C_v - C_v$	1.320	520.0
$C_v - H_v$	1.080	367.0

TABLE 2
Bond-angle variation parameters

Bond-angle variation	Θ (deg)	K^{θ} (kcal/mole/rad^2)
$C_t - C_t - C_t$	112.7	58.4
$C_t - C_t - H_t$	110.7	37.5
$C_t - C_t - O$	107.5	59.7
$H_t - C_t - H_t$	107.8	33.0
$H_t - C_t - O$	108.9	59.0
$C_v - C_v - H_v$	120.0	40.0
$C_v - C_v - C_a$	120.0	50.0
$H_v - C_v - H_v$	120.0	40.0
$H_v - C_v - C_a$	120.0	40.0
$C_v - C_a - C_a$	120.0	50.0
$C_a - C_a - C_a$	120.0	63.0
$C_a - C_a - H_a$	120.0	35.0
$C_a - C_a - O$	121.9	43.2
$C_t - O - C_a$	108.9	49.6

TABLE 3
Van der Waals interaction parameters

Van der Waals interaction	D^I (kcal/mole)	ρ^I (Å)
C_t	0.066	3.50
H_t	0.030	2.50
O	0.140	2.90
C_a	0.070	3.55
H_a	0.030	2.42
C_v	0.076	3.55
H_v	0.030	2.42

TABLE 4
Effective fiber independent parameters and elastic stiffness components

G_T^f = 4.4 GPa	C_{11}^f = 457.6 GPa
K_T^f = 9.9 GPa	C_{12}^f = 8.4 GPa
G_L^f = 27.0 GPa	C_{22}^f = 14.3 GPa
E_L^f = 450.4 GPa	C_{23}^f = 5.5 GPa
	C_{44}^f = 27.0 GPa

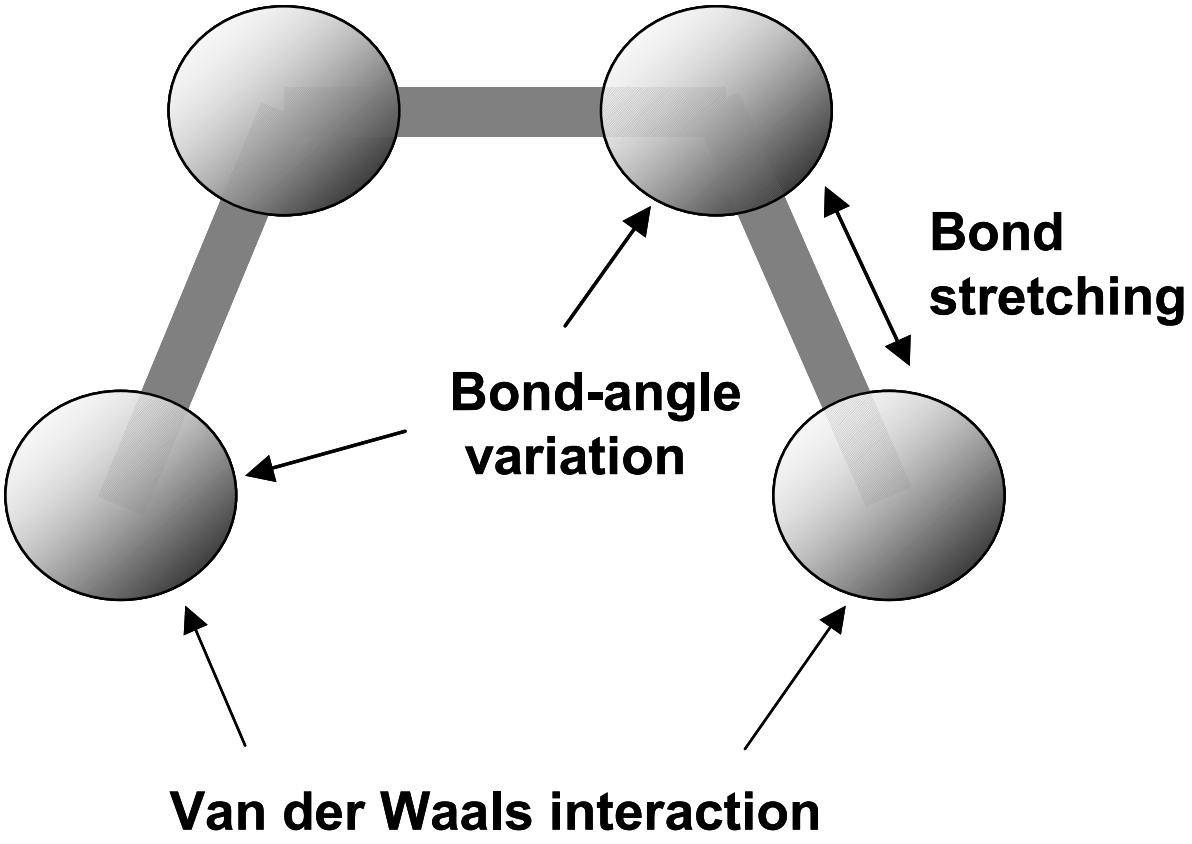

FIG. 1. *Molecular mechanics modeling*

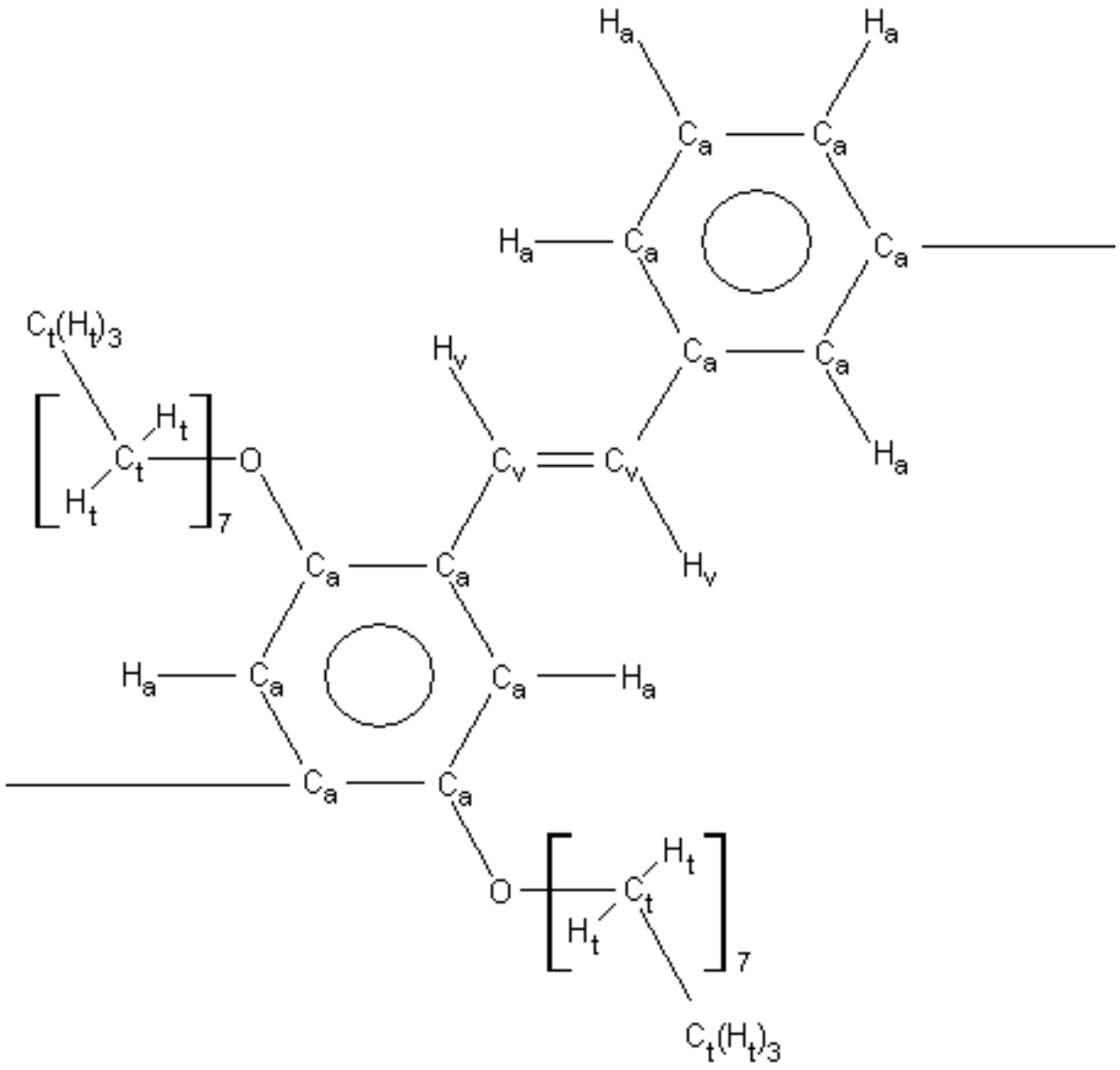

FIG. 2. *PmPV molecular structure*

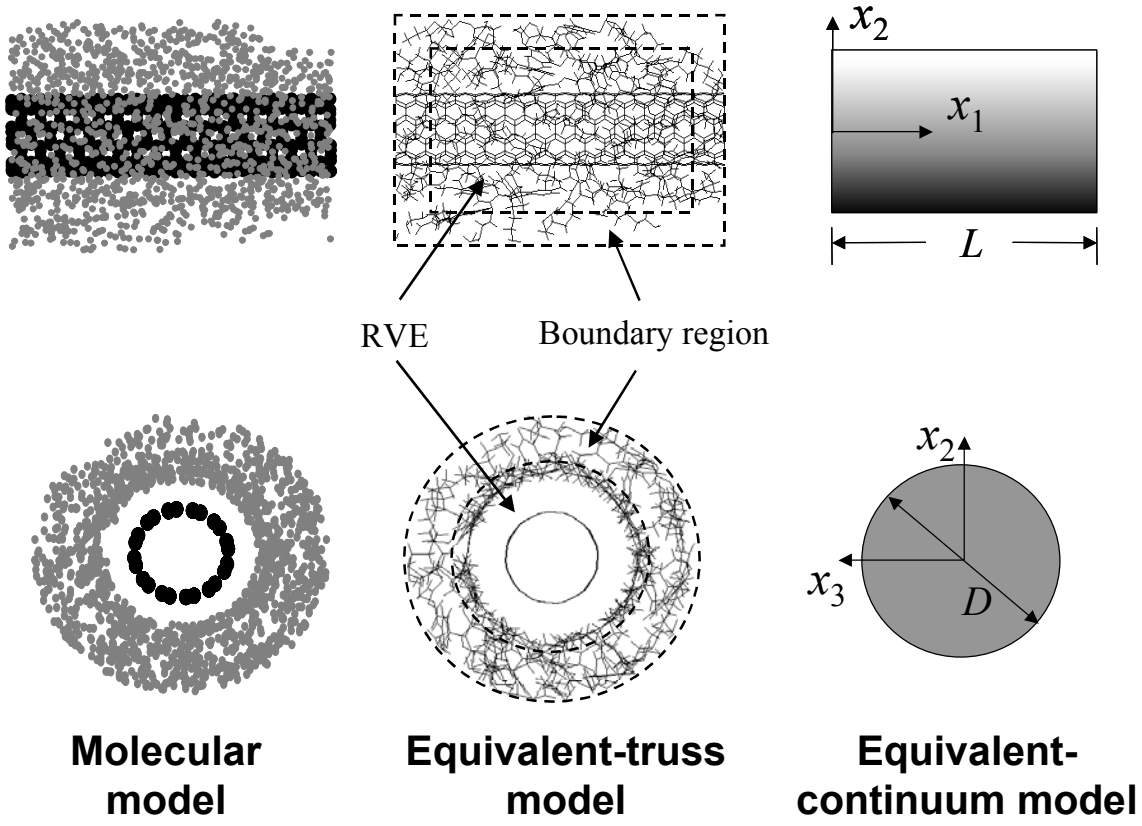

FIG. 3. *Equivalent-continuum modeling of effective fiber*

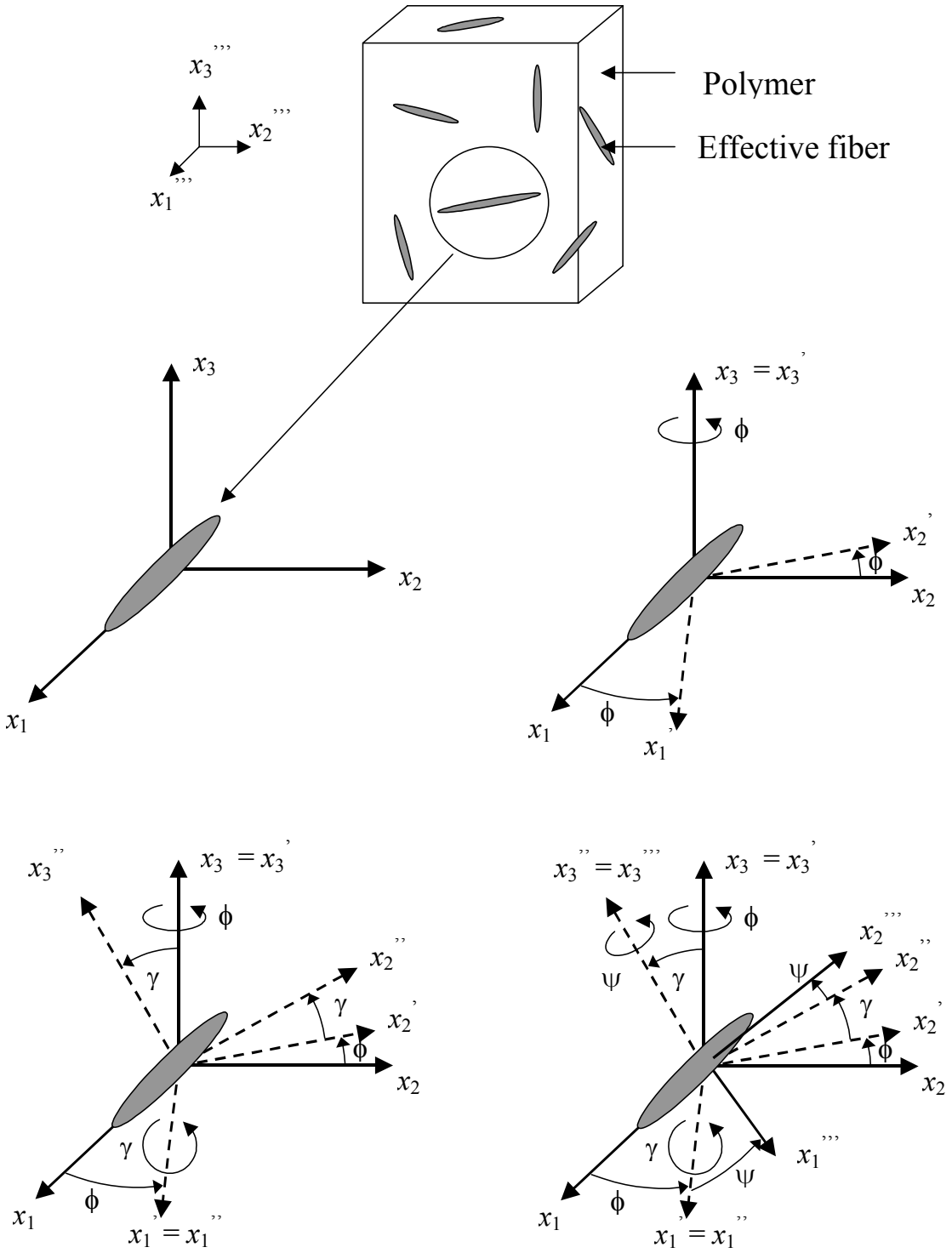

FIG. 4. *Effective fiber orientation*

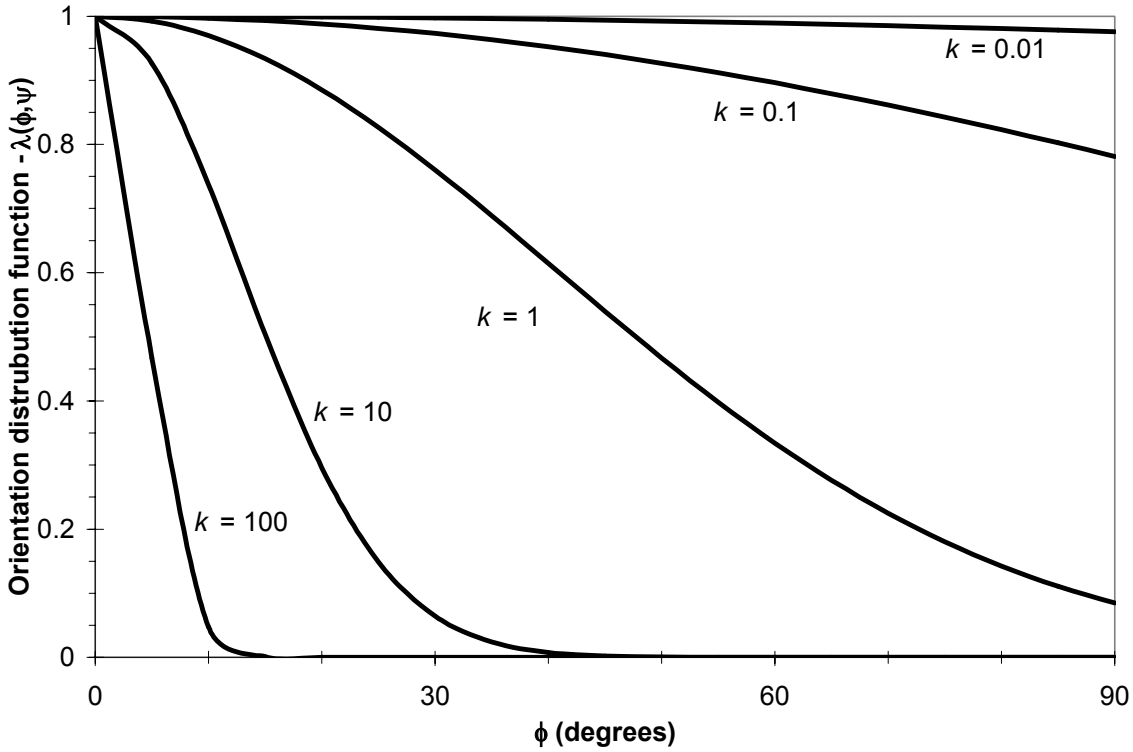

FIG. 5. *Orientation distribution function for various values of the alignment factor k*

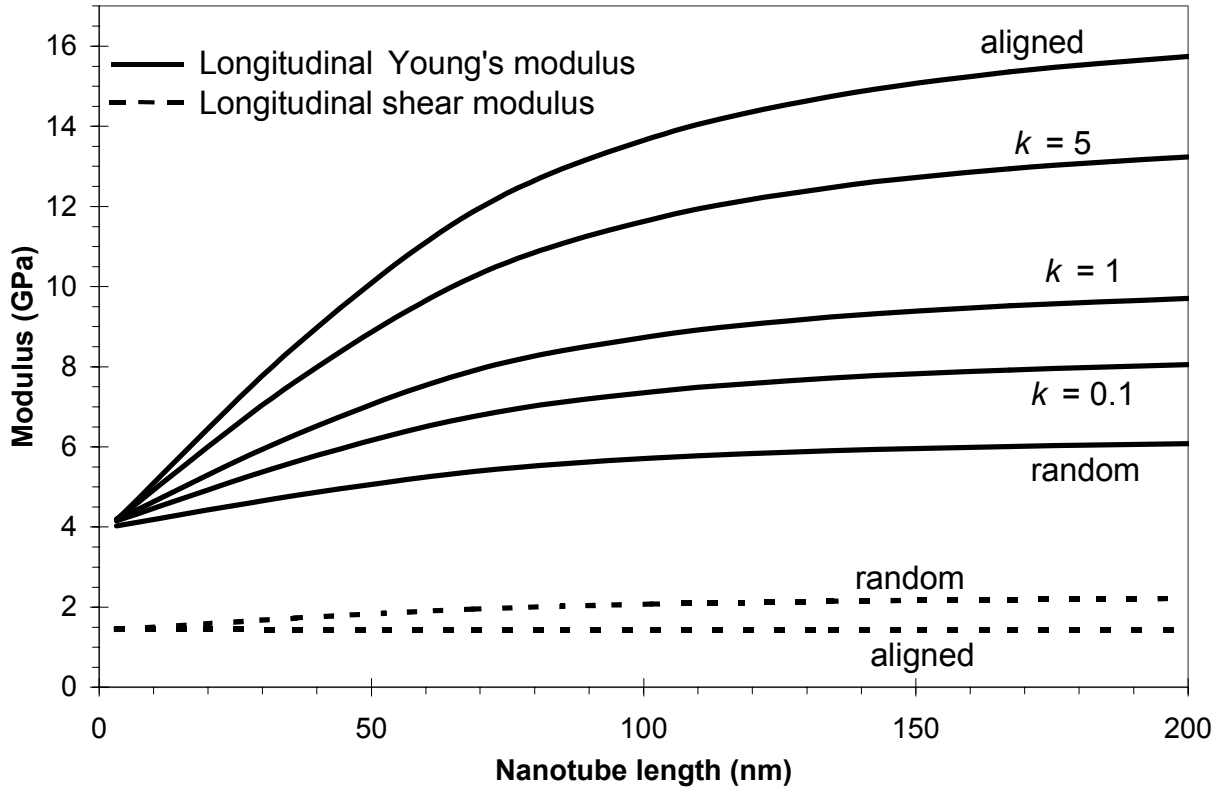

FIG. 6. *Modulus of SWNT/LaRC-SI composite material vs. nanotube length for a 1% nanotube volume fraction*

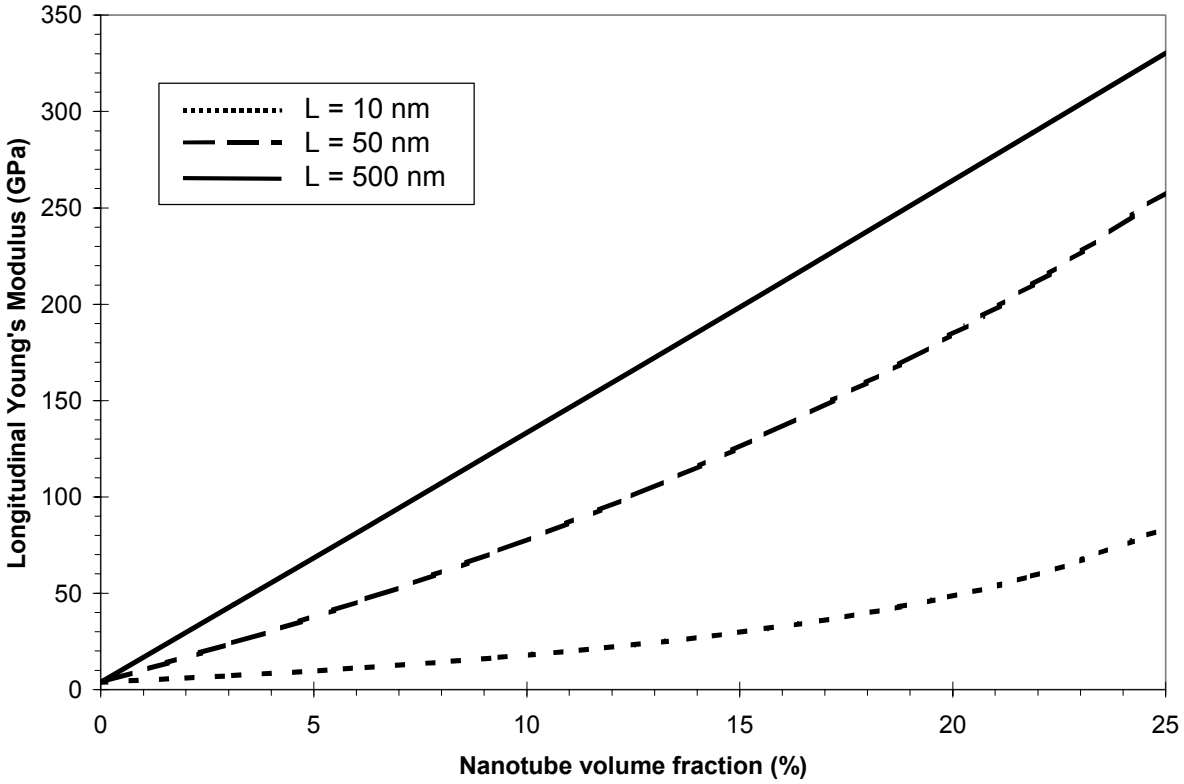

FIG. 7. *Longitudinal Young's modulus of aligned SWNT/LaRC-SI composite vs. nanotube volume fraction*

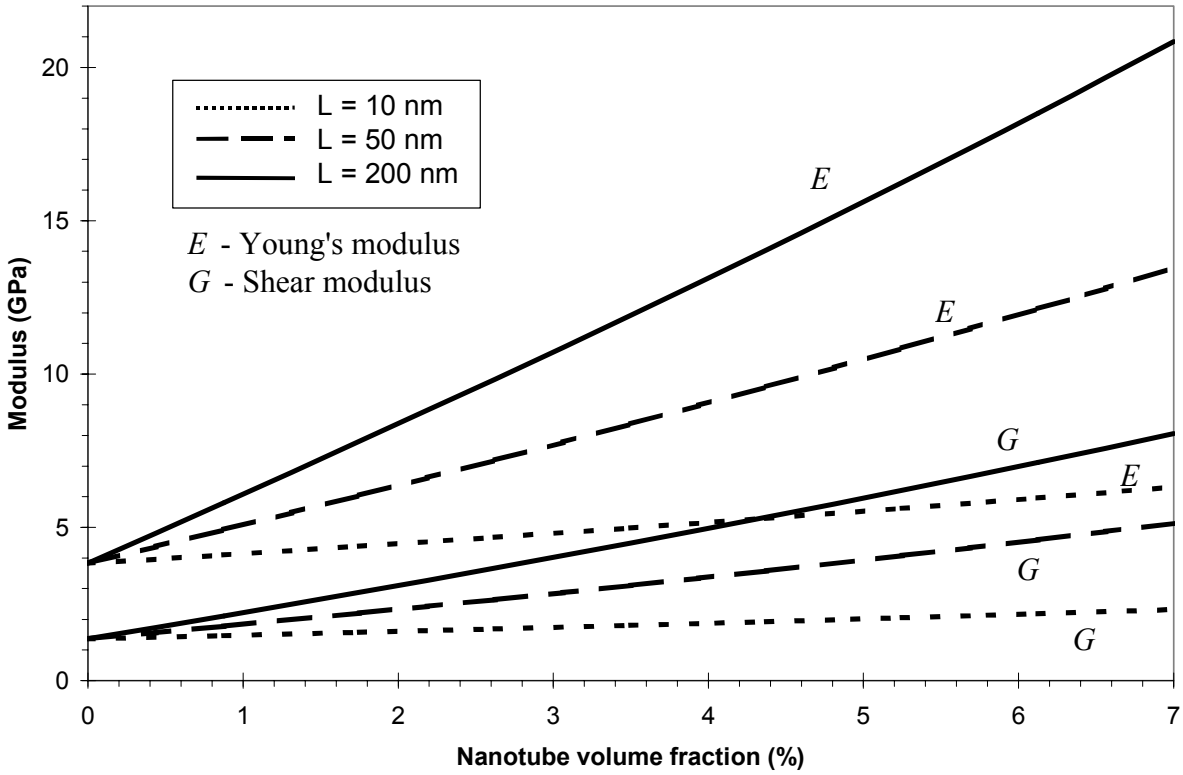

FIG. 8. *Modulus of random SWNT/LaRC-SI composite material vs. nanotube volume fraction*

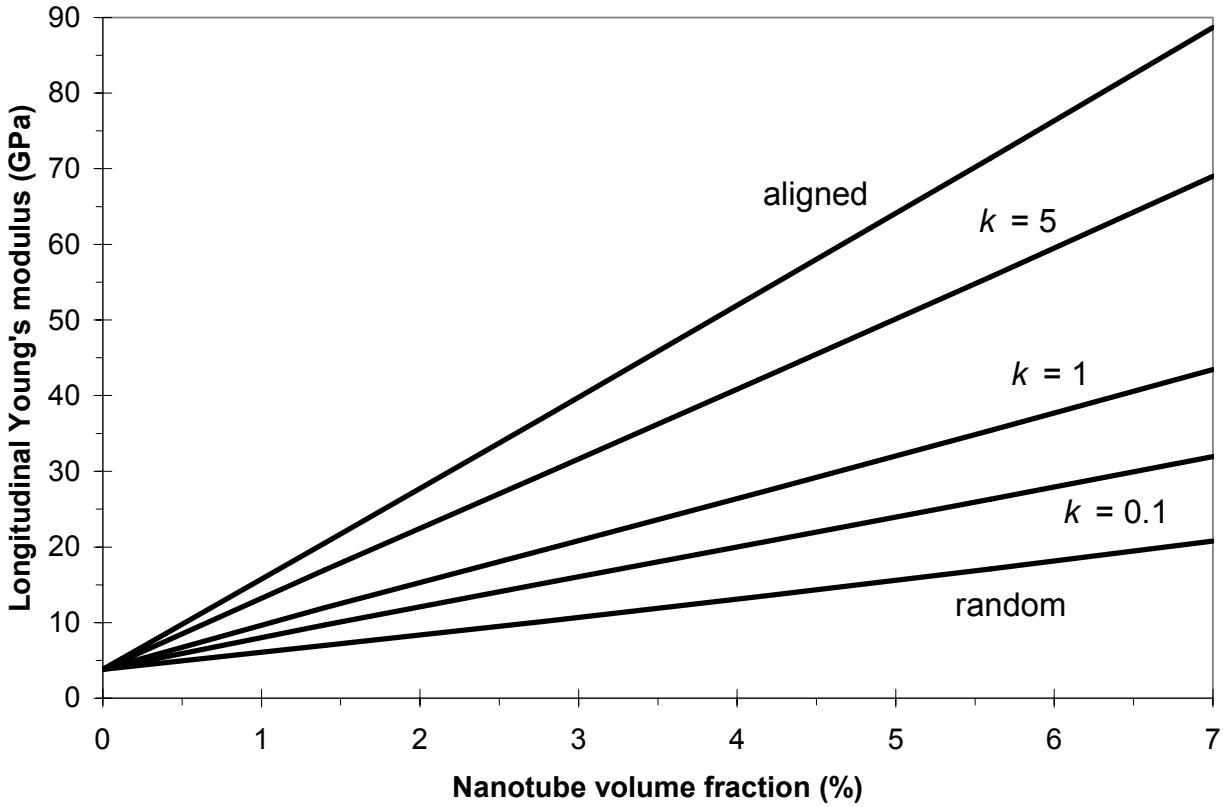

FIG. 9. *Longitudinal Young's modulus of axisymmetric SWNT/LaRC-SI composite material vs. nanotube volume fraction for nanotube lengths of 200 nm*

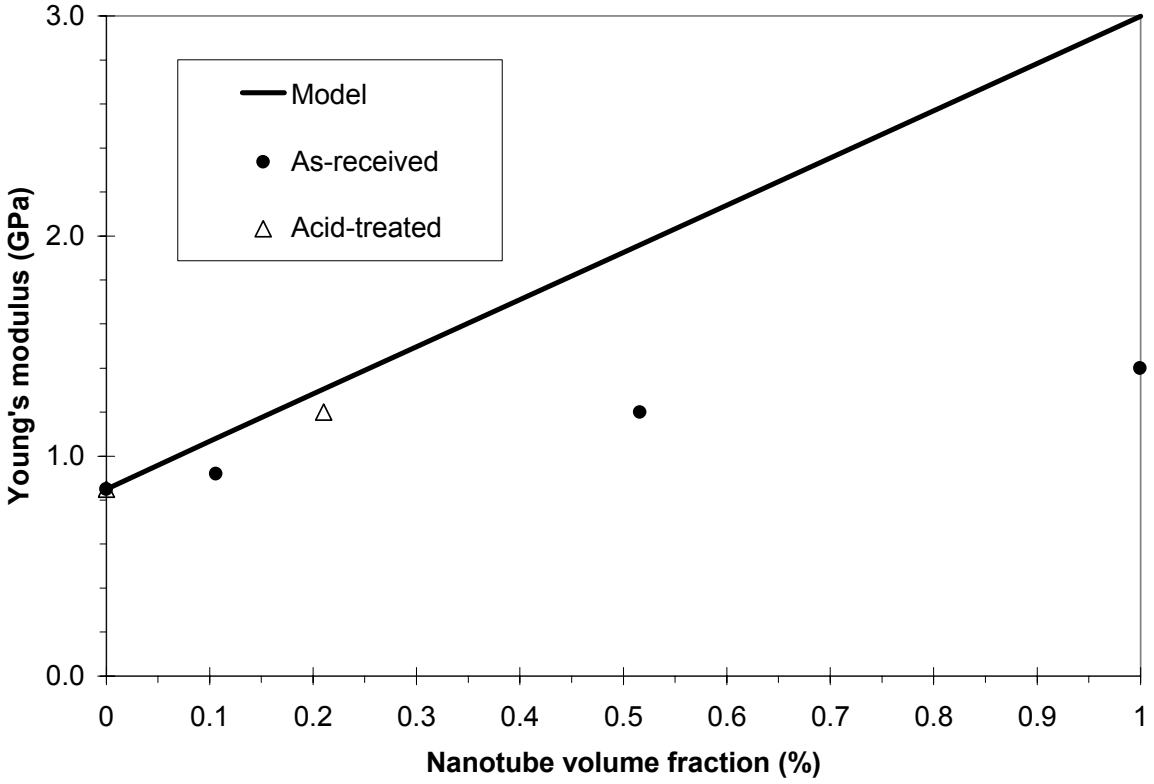

FIG. 10. *Young's modulus of random SWNT/LaRC-CP2 composite vs. nanotube volume fraction*

REPORT DOCUMENTATION PAGE

Form Approved
OMB No. 0704-0188

1. AGENCY USE ONLY *(Leave blank)*	2. REPORT DATE	3. REPORT TYPE AND DATES COVERED
	July 2002	Contractor Report

4. TITLE AND SUBTITLE
Constitutive modeling of nanotube-reinforced polymer composites

5. FUNDING NUMBERS
C NAS1-97046
WU 505-90-52-01

6. AUTHOR(S)
G.M. Odegard, T.S. Gates, K.E. Wise, C. Park, and E.J. Siochi

7. PERFORMING ORGANIZATION NAME(S) AND ADDRESS(ES)
ICASE
Mail Stop 132C
NASA Langley Research Center
Hampton, VA 23681-2199

8. PERFORMING ORGANIZATION REPORT NUMBER
ICASE Report No. 2002-27

9. SPONSORING/MONITORING AGENCY NAME(S) AND ADDRESS(ES)
National Aeronautics and Space Administration
Langley Research Center
Hampton, VA 23681-2199

10. SPONSORING/MONITORING AGENCY REPORT NUMBER
NASA/CR-2002-211760
ICASE Report No. 2002-27

11. SUPPLEMENTARY NOTES
Langley Technical Monitor: Dennis M. Bushnell
Final Report
Submitted to Composites Science and Technology.

12a. DISTRIBUTION/AVAILABILITY STATEMENT
Unclassified–Unlimited
Subject Category 34
Distribution: Nonstandard
Availability: NASA-CASI (301) 621-0390

12b. DISTRIBUTION CODE

13. ABSTRACT *(Maximum 200 words)*
In this study, a technique is presented for developing constitutive models for polymer composite systems reinforced with single-walled carbon nanotubes (SWNT). Because the polymer molecules are on the same size scale as the nanotubes, the interaction at the polymer/nanotube interface is highly dependent on the local molecular structure and bonding. At these small length scales, the lattice structures of the nanotube and polymer chains cannot be considered continuous, and the bulk mechanical properties can no longer be determined through traditional micromechanical approaches that are formulated by using continuum mechanics. It is proposed herein that the nanotube, the local polymer near the nanotube, and the nanotube/polymer interface can be modeled as an effective continuum fiber using an equivalent-continuum modeling method. The effective fiber serves as a means for incorporating micromechanical analyses for the prediction of bulk mechanical properties of SWNT/polymer composites with various nanotube lengths, concentrations, and orientations. As an example, the proposed approach is used for the constitutive modeling of two SWNT/polyimide composite systems.

14. SUBJECT TERMS
carbon nanotubes, composites, mechanical properties, modeling, nanotechnology

15. NUMBER OF PAGES
36

16. PRICE CODE
A03

17. SECURITY CLASSIFICATION OF REPORT	18. SECURITY CLASSIFICATION OF THIS PAGE	19. SECURITY CLASSIFICATION OF ABSTRACT	20. LIMITATION OF ABSTRACT
Unclassified	Unclassified		